

Industrial applications at the new cold neutron radiography and tomography facility of the HMI

N. Kardjilov^{*}, A. Hilger, I. Manke, M. Strobl, W. Treimer, J. Banhart

Hahn-Meitner-Institut Berlin, Glienicker Str. 100, D-14109 Berlin

Elsevier use only: Received date here; revised date here; accepted date here

Abstract

The new cold neutron radiography and tomography facility at the Hahn-Meitner-Institut Berlin is suited for the investigation of components and materials from different industrial fields. The high-flux measuring position of the facility allows real-time imaging of fast dynamical processes. Cold neutrons interact with a higher probability with the matter compared to thermal neutrons which leads to a much better radiography contrast. Some examples of different industry applications like investigations on discharging of a Lithium battery or on oil sediments in a vent pipe are presented.

PACS: 87.59.Fm

Keywords: neutron tomography, real-time radiography, industrial applications, battery

1. Introduction

In modern industry neutron tomography and radiography are of increasing interest and are used for investigations of industrial components and materials since many years [1-6]. Because of the unique properties of neutrons, tomography and radiography with neutrons are of special interest for automotive and aviation industry. The possibility to penetrate even several centimeters of metal on the one hand and the sensitivity to some light elements on the other hand provides high contrasts in images of metal components containing oils, plastics, adhesives etc.

At the Hahn-Meitner-Institut Berlin a new cold neutron radiography and tomography facility is under construction intended mainly for the needs of industry [7]. The instrument provides a high variability for different demands at two measuring positions, see Fig. 1. The first high-flux position is already in operation, while the second high-resolution position is under construction. At the first one a very high neutron flux of at least 10^9 neutrons/(cm²s) is available. This gives several advantages:

1. The time needed to take a tomography can be reduced. Therefore, investigations of fast processes, like a running machines or fast chemical reactions, are possible.
2. Cold neutrons increase the contrast between different materials.

^{*} Corresponding author. Tel.: +4930-8062-2298; fax: +4930-8062-3059; e-mail: kardjilov@hmi.de.

3. It allows the investigation of rather thick components, because of the enlarged dynamic range of the radiography image.

2. Experimental Setup

The new neutron radiography beam line at HMI V7 is placed at the end of the curved neutron guide NL1b facing the cold source of the BER-II reactor [7]. The existence of a neutron guide helps to achieve an enormous high cold neutron flux in the order of ca. 3×10^9 n/cm²s at the end position with a negligible background of gammas and fast neutrons. A measure for the level of the beam collimation is the so-called L/D ratio, described in more details elsewhere [8], where the larger the ratio the better is the beam collimation. The image quality depends directly on the beam collimation. At the first measuring position the L/D value is limited by the energy-dependant divergence produced from the guide. In case of a cold neutron beam it is measured in the order of 70 for a Ni coated guide [8] which provides a geometrical unsharpness of 250 μ m at a distance of 2 cm from the detector screen.

At the second position, see Fig. 1, an additional collimation system, consisted of a flight tube of 5 m length and a set of diaphragms, will be installed. This way the L/D value for the second measuring position will be increased to about of 500 and the spatial resolution will be improved down to 100 μ m.

The used detector system is based, for the moment, on a 12-bit interline-transfer CCD camera Sencam 1280x1024 pixels with a triggering option allowing exposure times down to 1 ms for real-time radiography. The image obtained by the LiZnS scintillator is projected via a mirror and a lens system onto the CCD chip giving a projection ratio of 26 μ m/pixel.

3. Experimental Results

The presented experiments below were performed at the first high-flux measuring position, where samples with small sizes (maximal beam size 3×5 cm²) can be investigated at a high neutron flux of $\sim 3 \times 10^9$ n/cm²s.

3.1. Lithium batteries

Because of the low specific weight, Lithium is widely used in the battery industry. Furthermore Lithium possesses one of the highest attenuation coefficients for cold neutrons among all the elements of ca. 11.7 cm⁻¹. Hence the Lithium batteries are interesting objects for investigations with neutron tomography, because the contrast to other battery components is very high [4,9].

Normally the content of a battery is gel-like because of the liquid ingredients i.e. the electrolyte. Thus, if cropped the surface pattern is blurred, even if the battery is frozen with liquid nitrogen.

The task to investigate a LiI battery with dimensions 2.6x2.8x0.3 cm³ by a neutron tomography method was a challenge for the recently established tomography facility at HMI. To perform a good tomography reconstruction a set of equidistance sample projections around a 180° angular interval are needed. This means that for some of the projections the neutron transmission should succeed for a LiI thickness of app. 2.6 cm.

The expected transmission of the beam in these cases was estimated to ? % which is considerably lower in comparison to the transmission of the transversal direction of the battery of 0.3 cm giving a transmission of 25%. Such a strong difference in the transmission at different projection angles usually leads to undesired artefacts in the tomography reconstruction.

To improve the signal-to-noise ratio for the projections with a bad neutron transmission several images were collected for every angle position. After adding up all of them a final projection image for the corresponding angle was obtained. The set of final projection images was tomographically reconstructed using a standard back-projection algorithm.

The number of the collected projections in the 180° angular interval was 200 which corresponds to an angular rotation step of 0.9°. For each angular position 50 images with an exposure time of 0.3 s were recorded and summed up to form a final image for the sample projection under this angle. After the summation the obtained final projections possessed an image dynamic of 32-bit grey levels, which is better than the recorded 12-bit single images.

The reconstruction algorithm was implemented in a self written IDL[®] [11] routine where the projections were normalized and prepared for tomography algorithm. After the tomography reconstruction the obtained 3D matrix was visualized by the 3D viewer software VG Studio[®] [12].

Figure 2 shows cross sections of a neutron tomography of a Lithium-Iodine-battery intended for a pacemaker device. The two pictures in figure 2 represents a tomography slice through the battery before (fig. 2 left) and after (fig. 2 right) discharging the battery for about 1 month.

This type of battery is made up of several coplanar plates of Lithium and Iodine. Normally it should last up to ten years. To discharge the battery more quickly it has been attached to a 200 k Ω resistor. But it still needs about 6 months to fully discharge the battery.

After the first month an unexpected dramatic change in the Lithium distribution can be observed. Before discharging, the Lithium distribution (white colored) is relatively smooth as it was expected from the manufacturing specifications. After discharging, the Lithium distribution is no longer smooth, but characterized by strong discontinuities. This is an evidence for a significant material transport in the electrolyte, caused by the chemical reaction between Lithium and Iodine.

This can also be seen in the 3D view in Figure 3. This figure shows the neutron tomography of a used Lithium-Iodine battery of a similar type. In this image the battery stainless steel case is rendered as transparent and the pure Lithium distribution is visible. The Lithium is arranged around a lattice-like vertical structure, that is typical for this type of battery

In addition to the analysis of chemical processes inside the battery the identification of manufacture errors or defects are of great importance. In figure 4 the case of the battery from figure 3 is shown, while the Lithium is transparent. In the sliced tomography some holes inside the case are visible ascribed to the manufacture process. Apparently the filling process does not work properly.

The results of this investigation may help increase the life-time of LiI batteries used in pacemakers.

3.2. Oil sediments in steel tubes

An example, illustrating the advantages of neutron tomography can be seen in Figure 5. A steel tube containing graphite powder has been investigated as a test sample. Conventional radiography or tomography with X-rays show nearly no contrast, because of the high attenuation coefficient of steel and the comparably low one for the graphite powder inside. Using neutron tomography the graphite distribution can be separated from the steel material very well.

To verify the resolution of the experimental setup, three pencil leads with 0.3, 0.5 and 0.7 mm diameter have been fixed inside the tube. The two thicker pencil leads can be seen, while the thinner one is below the resolution limit of the detector. In this case the sample was investigated at a larger distance from the detector of 5 cm, providing a larger geometrical unsharpness than the mentioned above 250 μm .

What has been demonstrated with this test sample, can be applied on steel or aluminum tubes widely used in industry. A vent pipe containing some minor sediments of soot and oil has been investigated. A radiography is shown in Figure 6. The small bright spots around the knee of the sample are caused by the high beam attenuation in the hydrogenous based soot-oil mixture.

Figure 7 shows a tomographic 3D view of the vent pipe and the sediments (dark marked). The volumes of the sediments were quantified using the classification tool of the 3D rendering software VG Studio[®]. They were estimated to be 0.6 mm³ and 8.1 mm³ correspondingly.

Such kind of investigations are very important for some safety inspections in the air craft or automotive industry.

3.3. Real-time radiography

The high flux at the new facility is also a precondition for real-time experiments, where fast processes are examined.

As a test sample an aluminum model air-craft combustion engine was investigated. The dimensions of the motor were 70.9x69.7x31.4 mm³ (WxHxT) which fits well to the beam size of 30x50 mm². For the first tests the engine was driven by a coupled

electromotor. On the crankshaft of the engine an aluminum disk with a slit and a photo sensor around it were placed in order to produce an exact trigger signal for the camera system.

The collection of the data was based on the so-called stroboscopic method at repetition processes. In this case an image set is recorded exactly at the same time point of the repetition process. After adding up of all the images for the corresponding time point, an average snapshot image with a better statistics was obtained. Using the time delay option of the camera software the whole combustion cycle was visualized by such “frozen” snapshot images.

The experiment was performed with a rotation speed of the engine of 1110 rpm which corresponds to a mean linear velocity of the piston of 0.5 m/s at a piston displacement of 27.2 mm per stroke. The exposure time was set to 1 ms which determines an image blur due to the piston movement of 500 μm . For a defined piston position (time point) 200 images were recorded. The time delay between two piston positions was set to 1 ms. The image processing was performed by a self written IDL routine where after correction and normalization of the collected images the average snapshot images were calculated.

Two snapshot images at different times are shown in Fig. 8. As seen from the images the statistics of the resultant images is good and image quality allows to recognize some details as the exhaust entrance seen as a bright area in the middle of the cylinder.

The next step in this work will be to investigate the fuel injection in a running motor driven by a combustion process.

4. Conclusion

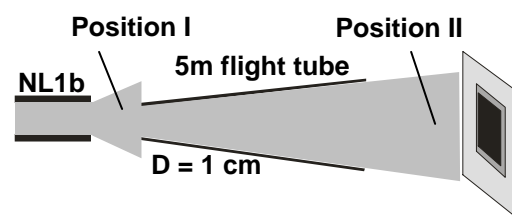
The experimental parameters and some industrial applications of the new radiography and tomography facility at Hahn-Meitner-Institut Berlin were presented.

The flexibility of the experimental setup and the high flux of more than 10^9 neutrons/(cm^2s) will be used in the future for a various industrial applications.

Some first examples demonstrating the advantages of this new facility were shown.

5. References

- [1] A.C. Kak, M. Slaney, Principals of Computerized Tomographic Imaging, IEEE Press, New York, 1987
- [2] J.C. Domanus (Ed.), Practical Neutron Radiography, Kluwer Academic Publishers, Dordrecht, The Netherlands, 1992
- [3] B. Schillinger, E. Lehmann, P. Vontobel, Physica B, 276-278 (2000), p. 59-62
- [4] M. Lanz, E. Lehmann, W. Scheifele, R. Imhof, I. Exnar, P. Novák, Journal of Power Sources 101 (2001), p. 177-181
- [5] E.H. Lehmann, P. Vontobel, N. Kardjilov, Applied Radiation and Isotopes 61 (2004), p. 503-509
- [6] I. Manke, N. Kardjilov, R. Schneider, A. Haibel, A. Denker, A. Rack, A. Hilger und J. Banhart, ZfP-Zeitung 88 (2004), p. 31-40
- [7] N. Kardjilov, A. Hilger, M. Dierik, B. Masschaele, BENSIC Experimental Reports 2003, ISSN 0936-0891
- [8] B. Schillinger, Nondestr. Test. Eval. 16 (2001), p. 141
- [9] D. Goers, M. Holzapfel, W. Scheifele, E. Lehmann, P. Vontobel, P. Novák, Journal of Power Sources 130 (2004), p. 221-226



Position I (high flux)

(in operation):

Neutron flux: 3×10^9 n/cm²s

Beam size: 3×5 cm²

Collimation ratio (L/D): 70

Spatial resolution: $\sim 250 \mu\text{m}$

Position II (high resolution)

(under construction):

Neutron flux: $\sim 10^7$ n/cm²s

Beam size: 15×15 cm²

Collimation ratio (L/D): 500

Spatial resolution: $\sim 100 \mu\text{m}$

Fig. 1: Schematic layout of the radiography facility at HMI

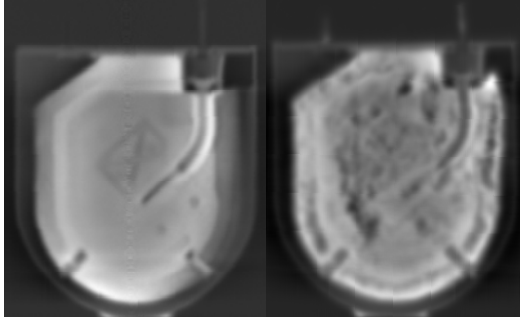


Fig. 2: Cross sections of a tomography of a Lithium-Iodine battery before (left) and after (right) discharging. The material with high attenuation coefficient i.e. the Lithium is white.

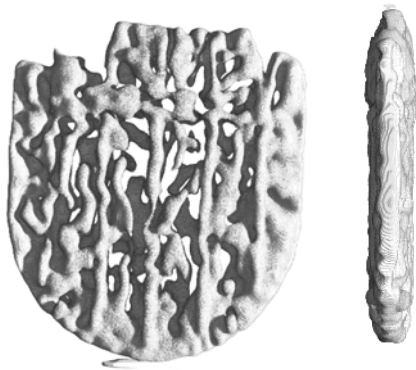


Fig. 3: Because of the high mass attenuation coefficient the Lithium can be separated from other battery components very well, thus the Lithium distribution becomes visible.

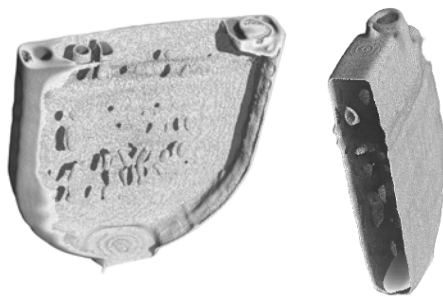


Fig. 4: Neutron tomography of the Lithium battery. The sliced case and some holes inside are visible. The other parts are not shown.



Fig. 5: Neutron tomography of a steel pipe containing some toner of a laser printer and two pencil leads with 0.7 and 0.5 mm in diameter. The toner distribution as well as the pencil leads can be seen.

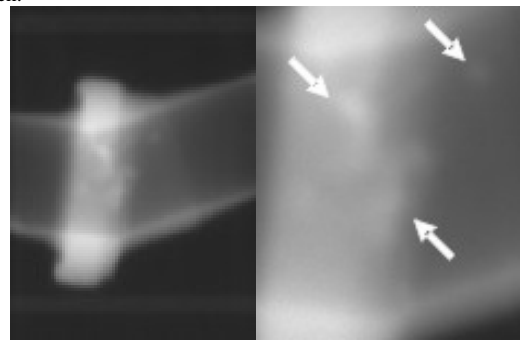


Fig. 6: Left: Neutron Radiography of a vent pipe made of steel containing small amounts of a mixture of soot and oil. Right: Enlargement of the area, where the soot can be seen.

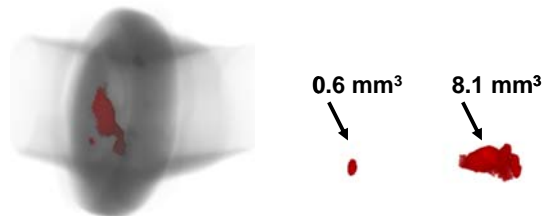


Fig. 7: Left: Neutron tomography of the steel pipe shown in Fig. 6. Right: The contaminations inside the tube have been separated for further investigations.

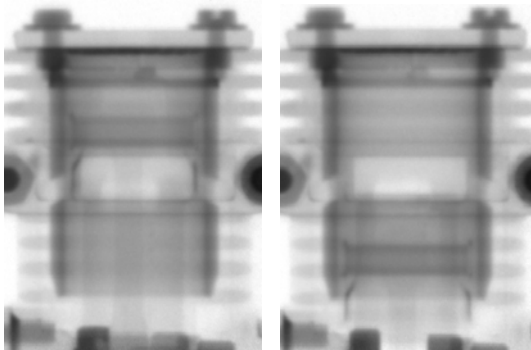


Fig. 8: Radiography of a running model aircraft engine (Left: Piston in the upper position, Right: Piston in the lower position). Because of the high flux the moving piston can be observed with an exposure time of 1 ms. The quality of the picture above has been enhanced by stroboscopic addition of several radiographies.